

Implicit Image-to-Image Schrödinger Bridge for CT Super-Resolution and Denoising

Yuang Wang^{1,2}, Siyeop Yoon², Pengfei Jin², Matthew Tivnan², Zhenhong Chen², Rui Hu^{2,3}, Li Zhang¹, Zhiqiang Chen¹, Quanzheng Li², and Dufan Wu^{2*}

¹ Department of Engineering Physics, Tsinghua University, Beijing, China

² Department of Radiology, Massachusetts General Hospital and Harvard Medical School, Boston, USA

³ Zhejiang University, Zhejiang, China

Abstract. Conditional diffusion models have gained recognition for their effectiveness in image restoration tasks, yet their iterative denoising process, starting from Gaussian noise, often leads to slow inference speeds. As a promising alternative, the Image-to-Image Schrödinger Bridge (I²SB) initializes the generative process from corrupted images and integrates training techniques from conditional diffusion models. In this study, we extended the I²SB method by introducing the Implicit Image-to-Image Schrödinger Bridge (I³SB), transitioning its generative process to a non-Markovian process by incorporating corrupted images in each generative step. This enhancement empowers I³SB to generate images with better texture restoration using a small number of generative steps. The proposed method was validated on CT super-resolution and denoising tasks and outperformed existing methods, including the conditional denoising diffusion probabilistic model (cDDPM) and I²SB, in both visual quality and quantitative metrics. These findings underscore the potential of I³SB in improving medical image restoration by providing fast and accurate generative modeling.

Keywords: Schrödinger bridge · Super resolution · Denoising.

1 Introduction

Restoration of high-quality images accurately from corrupted inputs is a common and challenging task in medical imaging processing such as denoising and super-resolution. In recent years, conditional diffusion models[10,12] have demonstrated promising performance in tackling this task. Based on stochastic process theories, diffusion models provide a more stable solution to sample from complex distributions compared to Generative Adversarial Networks (GANs)[14]. However, diffusion models suffer from slow inference speed due to the large number of iterative denoising steps required to generate clean images starting from pure Gaussian noise.

* Corresponding author: dwu6@mgh.harvard.edu

Instead of starting from Gaussian noise, Schrödinger bridges[2,3,5] establish diffusion bridges between the distributions of clean and corrupted images. By initiating the diffusion process with the corrupted image that is closer to the clean one compared to Gaussian noise, Schrödinger bridges provide a promising approach to generate high-quality conditional samples with fewer diffusion steps. As a special case, the Image-to-Image Schrödinger Bridge (I²SB)[11] models the diffusion bridge between paired clean-corrupted samples, and enables efficient training through connecting it with the standard score-based diffusion model. Despite the reduction of the needed sampling steps compared to conventional diffusion models, it has been observed that I²SB tends to produce smoothed images[4] using small number of sampling steps, due to the so-called "regression to the mean effect"[6].

Inspired by the success of introducing non-Markovian process into the denoising diffusion probabilistic model (DDPM)[8] to formulate the denoising diffusion implicit model (DDIM)[13], we proposed a novel method, Implicit Image-to-Image Schrödinger Bridge (I³SB), which uses non-Markovian process during the inference of I²SB. The training process of the proposed I³SB is same with I²SB, but during testing, the initial corrupted image is incorporated in each step besides the current image and the estimated mean. A single parameter was proposed to balance between the Markovian (I²SB) and the non-Markovian (I³SB) components, which can be adjusted across the diffusion process for better image restoration. We validated the method on two image restoration tasks, including quarter-dose abdominal CT image denoising and 4× chest CT super-resolution. The proposed I³SB was compared to I²SB and conditional DDPM (cDDPM) and demonstrated improved texture restoration.

2 Method

Notation: Let $X_t \in R^d$ represent a d-dimensional stochastic process indexed by $t \in [0, 1]$, and N denote the number of generative steps. We denote the discrete generative time steps as $0 = t_0 < \dots < t_n \dots < t_N = 1$, and shorthand $X_n \equiv X_{t_n}$.

2.1 Image-to-Image Schrödinger Bridge

The I²SB establishes direct diffusion bridges between the clean image distribution A and the corrupted image distribution B . Assuming paired data can be obtained during training, with X_0 denoting the sample from distribution A and X_1 denoting the corresponding sample from distribution B , X_t is designed to follow the distribution $q(X_t|X_0, X_1)$:

$$q(X_t|X_0, X_1) = \mathcal{N}\left(X_t; \frac{\bar{\sigma}_t^2}{\bar{\sigma}_t^2 + \sigma_t^2}X_0 + \frac{\sigma_t^2}{\bar{\sigma}_t^2 + \sigma_t^2}X_1, \frac{\sigma_t^2\bar{\sigma}_t^2}{\bar{\sigma}_t^2 + \sigma_t^2}I\right), \quad (1)$$

where $\sigma_t^2 = \int_0^t \beta_\tau d\tau$ and $\bar{\sigma}_t^2 = \int_t^1 \beta_\tau d\tau$ represent variances accumulated from either side, and β determines the speed of diffusion. As X_t can be sampled analytically using equation (1), the network ϵ_θ can be efficiently trained to predict

the difference between X_t and X_0 by minimizing the loss function:

$$\theta^* = \arg \min_{\theta} E_{X_0, X_1, y} E_{t \sim \mathcal{U}[0,1], X_t \sim q(X_t|X_0, X_1)} \|\epsilon_{\theta}(X_t, t, y) - \frac{X_t - X_0}{\sigma_t}\|, \quad (2)$$

where y denotes any potential conditions.

In the generative process, I²SB begins with the corrupted image X_N and iteratively approaches the clean image X_0 . In the step from X_{n+1} to X_n , \hat{X}_0 , an approximation of X_0 , is first calculated using the trained network ϵ_{θ^*} and X_{n+1} :

$$\hat{X}_0 = X_{n+1} - \sigma_{n+1} \epsilon_{\theta^*}(X_{n+1}, t_{n+1}, y), \quad (3)$$

where we use $\sigma_n \equiv \sigma_{t_n}$. Subsequently, X_n is sampled from the DDPM posterior p using \hat{X}_0 and X_{n+1} :

$$X_n \sim p(X_n | \hat{X}_0, X_{n+1}). \quad (4)$$

Here, the DDPM posterior p is expressed as

$$p(X_n | X_0, X_{n+1}) = \mathcal{N}\left(X_n; \frac{\alpha_n^2}{\alpha_n^2 + \sigma_n^2} X_0 + \frac{\sigma_n^2}{\alpha_n^2 + \sigma_n^2} X_{n+1}, \frac{\sigma_n^2 \alpha_n^2}{\alpha_n^2 + \sigma_n^2} I\right), \quad (5)$$

where $\alpha_n^2 = \int_{t_n}^{t_{n+1}} \beta_{\tau} d\tau$ denotes the accumulated variance between consecutive time steps t_n and t_{n+1} . The DDPM posterior p satisfies the equation

$$q(X_n | X_0, X_N) = \int p(X_n | X_0, X_{n+1}) q(X_{n+1} | X_0, X_N) dX_{n+1}, \quad (6)$$

which guarantees that X_n sampled using equation (4) is exactly a sample from $q(X_n | X_0, X_N)$ assuming the trained network ϵ_{θ^*} is perfect.

2.2 Implicit Image-to-Image Schrödinger Bridge

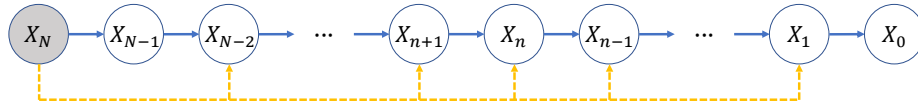


Fig. 1. Non-Markovian generative process of I³SB. Solid arrows denote original dependencies in I²SB, and dotted arrows signify additional dependencies in I³SB.

We preserve the training process of I²SB and modify its generative process in our proposed I³SB. The generative process of I²SB is essentially a Markovian process, as X_n is solely dependent on X_{n+1} given the trained network ϵ_{θ^*} and the condition y (\hat{X}_0 is also a function of X_{n+1}). I³SB is non-Markovian by conditioning X_n on both X_{n+1} and X_N , as shown in Fig. 1. In the generative

Algorithm 1 Generation Procedures of I³SB**Input:** $N, \{t_n\}, X_N \sim p_B(X_N)$, condition y , trained network ϵ_{θ^*}

```

for  $n = N$  to 1 do
  Predict  $\hat{X}_0$  using  $\epsilon_{\theta^*}(X_n, t_n, y)$ 
  if  $n == N$  then
    Sample  $X_{n-1}$  from  $p(X_{n-1}|\hat{X}_0, X_n)$ 
  else if  $1 < n < N$  then
    Sample  $X_{n-1}$  from  $p_G(X_{n-1}|\hat{X}_0, X_n, X_N)$ 
  else
     $X_0 = \hat{X}_0$ 
  end if
end for
return  $X_0$ 

```

step from X_{n+1} to X_n , we first compute \hat{X}_0 using equation (3) and then sample X_n from the distribution p_G :

$$X_n \sim p_G(X_n|\hat{X}_0, X_{n+1}, X_N), \quad (7)$$

where X_N is included. p_G should satisfy the equation:

$$q(X_n|X_0, X_N) = \int p_G(X_n|X_0, X_{n+1}, X_N) q(X_{n+1}|X_0, X_N) dX_{n+1}, \quad (8)$$

to guarantee that X_n sampled using equation (7) is precisely a sample from $q(X_n|X_0, X_N)$ assuming the trained network ϵ_{θ^*} is perfect. Assuming that p_G is a Gaussian distribution with a linear combination of X_0 , X_{n+1} and X_N as its mean, p_G can be expressed as

$$p_G(X_n|X_0, X_{n+1}, X_N) = \mathcal{N}(X_n; A_n X_0 + B_n X_{n+1} + C_n X_N, g_n^2 I), \quad (9)$$

where A_n , B_n and C_n represent the weights of X_0 , X_{n+1} and X_N , respectively, and $g_n^2 I$ is the variance of p_G . Substituting equation (9) into equation (8), the weights A_n , B_n and C_n can be analytically expressed in terms of g_n :

$$A_n = \frac{\bar{\sigma}_n^2}{\sigma_n^2 + \bar{\sigma}_n^2} - \frac{\bar{\sigma}_{n+1}^2}{\sigma_{n+1}^2 + \bar{\sigma}_{n+1}^2} \frac{\sqrt{\sigma_n^2 \bar{\sigma}_n^2 - g_n^2 (\sigma_n^2 + \bar{\sigma}_n^2)}}{\sigma_{n+1} \bar{\sigma}_{n+1}}, \quad (10)$$

$$B_n = \frac{\sqrt{\sigma_n^2 \bar{\sigma}_n^2 - g_n^2 (\sigma_n^2 + \bar{\sigma}_n^2)}}{\sigma_{n+1} \bar{\sigma}_{n+1}}, \quad (11)$$

and

$$C_n = \frac{\sigma_n^2}{\sigma_n^2 + \bar{\sigma}_n^2} - \frac{\sigma_{n+1}^2}{\sigma_{n+1}^2 + \bar{\sigma}_{n+1}^2} \frac{\sqrt{\sigma_n^2 \bar{\sigma}_n^2 - g_n^2 (\sigma_n^2 + \bar{\sigma}_n^2)}}{\sigma_{n+1} \bar{\sigma}_{n+1}}. \quad (12)$$

Consequently, p_G can be expressed analytically, and X_n can be efficiently sampled using equation (7). The generation procedures of I³SB are summarized in Algorithm 1.

The term g_n can be designed freely, provided it adheres to the constraint:

$$g_n \leq \frac{\sigma_n \bar{\sigma}_n}{\sqrt{\sigma_n^2 + \bar{\sigma}_n^2}}, \quad (13)$$

to ensure the meaningfulness of taking the square root in equations (10), (11) and (12). When g_n equals to $\sigma_n \alpha_n / \sqrt{\sigma_n^2 + \alpha_n^2}$ for any n , p_G becomes equivalent to the DDPM posterior p , and the generative process of I³SB reverts to that of I²SB.

Notably, g_n may be changed at different steps during one sampling, to emphasize different contributions from \hat{X}_0 , X_{n+1} and X_N at different stage to encourage better image restoration. At early stage where n is closer to N , a larger g_n would emphasize $A_n \hat{X}_0$ but downplay $B_n X_{n+1} + C_n X_N$. It is desired given that X_{n+1} and X_N contains less information on the clean image than \hat{X}_0 . As n approaches 0, X_{n+1} starts to contain more information, and a smaller g_n is preferred to emphasize $A_n \hat{X}_0 + B_n X_{n+1}$ but suppress $C_n X_N$ alone.

Based on this rationale, we parameterized g_n with a simple step function:

$$g_n = k_n \frac{\sigma_n \alpha_n}{\sqrt{\sigma_n^2 + \alpha_n^2}}, \quad (14)$$

where

$$k_n = \begin{cases} 0, & \frac{n}{N} \leq r, \\ 1, & \frac{n}{N} > r, \end{cases} \quad (15)$$

where r is a hyperparameter ranging from 0 to 1.

2.3 Implementation Details

We validated our proposed model on both CT super-resolution and denoising tasks. For the CT super-resolution task, we utilized the RPLHR-CT-tiny dataset consisting of anonymized chest CT volumes[16]. The original CT images were considered high resolution (HR) and were downsampled by a factor of 4 in the projection domain to generate corresponding low-resolution (LR) images. 20 cases (6195 slices) were used for training and 5 cases (1425 slices) were used for testing. For the CT denoising task, we utilized the Mayo Grand Challenge dataset[1]. The dataset includes anonymized abdominal CT scans from 10 patients (5936 slices) with matched full-dose (FD) data and simulated quarter-dose (QD) data. We used 8 patients for training and 2 for testing in our experiment.

The neural network $\epsilon_\theta(X_n, t_n, y)$ is a 2D residual U-Net with the same architecture used in DDPM[8]. The condition y contains X_N and the positional encodings and is concatenated to X_n along the channel dimension. During training, we utilized 1000 diffusion time steps with quadratic discretization, and adopted

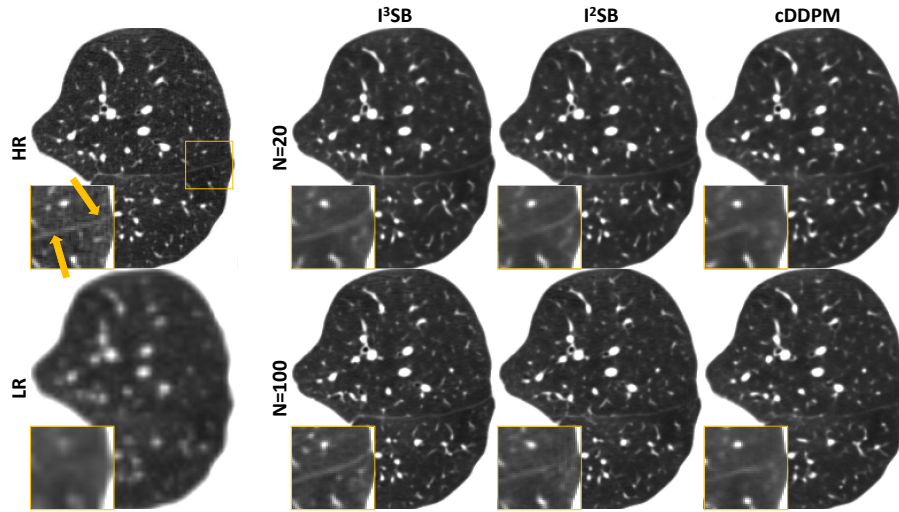


Fig. 2. Results from the $4\times$ chest CT super-resolution task. The restored anatomical features within the yellow box are zoomed in for enhanced visual clarity. The display window for the entire images is set to $[-1000, -250]$ HU, and for the zoomed regions is set to $[-1000, -550]$ HU.

Table 1. Quantitative results of tested methods for the CT super resolution task. For 1000 steps cDDPM, the normalized Haralick feature distance is 0.507 and SSIM is 0.9323.

N	Haralick (LR: 2.773)			SSIM (LR: 0.8757)		
	20	50	100	20	50	100
cDDPM	1.881	1.530	1.250	0.9492	0.9470	0.9443
I ² SB	1.679	1.218	0.908	0.9482	0.9442	0.9405
I ³ SB	1.596	1.103	0.780	0.9476	0.9429	0.9384

a symmetric scheduling of β_t with a maximum value of 0.15 at $t = 0.5$ [2,5]. The model was trained on randomly cropped patches of size 128×128 and tested on the entire 512×512 images. A batch size of 64 was employed during training, using the Adam algorithm with a learning rate of 8×10^{-5} for 200,000 iterations. The number of generative steps N was set to 20, 50, and 100, with r set to 0.2.

3 Results

We conducted a comparative analysis between our proposed I³SB, I²SB and cDDPM. Apart from selecting β_t according to the sigmoid schedule[9] in cDDPM, we maintained consistent network architecture and all training settings across all methods to ensure a fair comparison. Representative results are visualized in Fig. 2 and Fig. 3. A region containing a pulmonary fissure in the chest CT

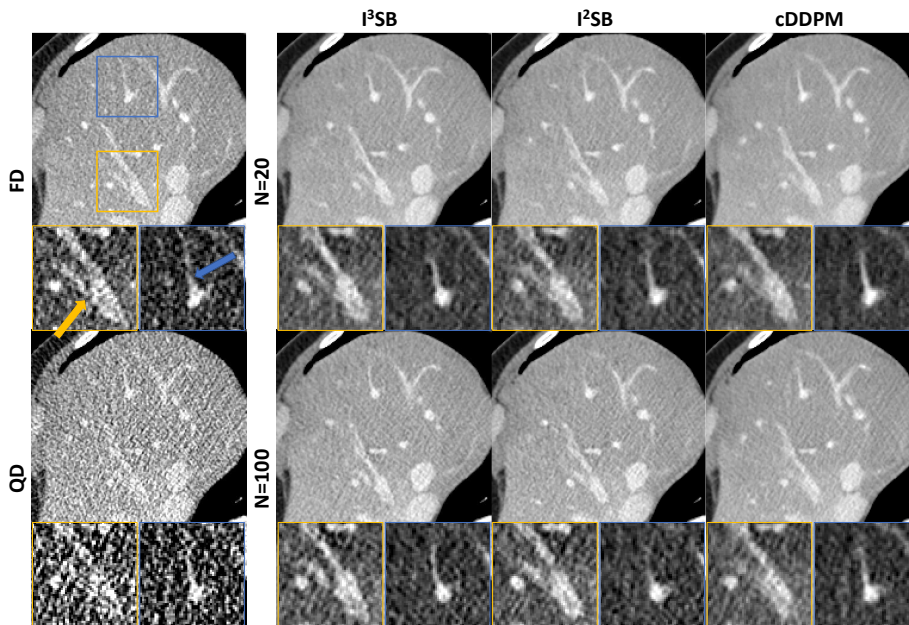


Fig. 3. Results from the quarter-dose abdominal CT denoising task. The restored anatomical features within the yellow and blue boxes are zoomed in for enhanced visual clarity. The display window for the entire images is set to $[-160, 240]$ HU, and for the zoomed regions is set to $[50, 230]$ HU.

images and two regions containing hepatic veins in the abdominal CT images are zoomed in for enhanced visual clarity. I^3SB and I^2SB have better texture recovery and less oversmoothing at both 20 and 100 steps for both tasks compared to cDDPM. Compared to I^2SB , I^3SB managed to recover the entire fissure with $N = 100$, where I^2SB showed broken ends using the same time steps at the location indicated by the yellow arrow in Fig. 2. I^3SB also has better recovery of the subtle vessel as pointed by the blue arrow as demonstrated in the $N = 100$ results in Fig. 3.

For quantitative assessment of the texture restoration ability of these models, we calculated normalized Haralick feature distances [7,15] within the external bounding box of the lungs for the chest CT dataset (window $[-1000, 200]$ HU) and within the external bounding box of the liver for the abdominal CT dataset (window $[-160, 240]$ HU). Additionally, to evaluate the models' fidelity to the ground truth, structural similarity index measures (SSIMs) were computed within the external bounding box encompassing the entire chest or abdomen (window $[-1000, 2000]$ HU). The quantitative results for the super resolution task are detailed in Table 1, and for the denoising task are detailed in Table 2.

Notably, the same tendency can be observed in both the CT super-resolution task and the CT denoising task. As N increases, the normalized Haralick feature

Table 2. Quantitative results of tested methods for the CT denoising task. For 1000 steps cDDPM, the normalized Haralick feature distance is 0.391 and SSIM is 0.9429.

N	Haralick (QD: 1.863)			SSIM (QD: 0.8731)		
	20	50	100	20	50	100
cDDPM	1.183	1.002	0.835	0.9539	0.9558	0.9541
I ² SB	0.953	0.736	0.594	0.9581	0.9544	0.9510
I ³ SB	0.924	0.693	0.540	0.9577	0.9535	0.9495

distances of both I²SB and I³SB become better, while the SSIMs worsen. This occurs because with an increased number of generative steps, these models tend to generate more details at the expense of some distortion from ground truth[4]. With the same number of generative steps, the SSIMs of cDDPM are negligibly better than those of I²SB and I³SB, with a difference of less than 0.5% for most of the cases, indicating that the three methods have similar level of fidelity of the restored images. However, cDDPM’s normalized Haralick feature distances are much worse, with relative increases from 15% to 60%. This is inline with our observation from Figs. 2 and 3 that cDDPM produces oversmoothing results compared to the other two. Compared with I²SB, our proposed I³SB achieves 5% to 10% better normalized Haralick feature distances with negligible worse SSIMs (<0.5%), suggesting that I³SB can generate more detailed images while maintaining consistency with ground truth established by I²SB.

4 Conclusion and Discussion

In conclusion, we proposed I³SB, a novel model that extends the generative process of I²SB to a non-Markovian process that incorporates corrupted images in each generative step. This innovation enables the generation of more detailed images without increasing distortion. Compared to I²SB and cDDPM, I³SB achieved similar fidelity but improved texture recovery in both CT super-resolution and denoising tasks. Furthermore, the hyperparameter g_n introduces flexibility into the inference of I²SB with almost no additional cost.

I³SB shows promise for further refinement in the design of g_n , which regulates stochastic uncertainty and the weighting of \hat{X}_0 , X_{n+1} , and X_N during image generation. While g_n is currently a simple step function of n , our future work aims to develop g_n as a function of \hat{X}_0 , X_{n+1} , X_N , and n . Additionally, we intend to integrate reinforcement learning into I³SB to enable g_n to adapt autonomously, potentially offering significant enhancements to our proposed model.

References

1. AAPM: Low dose ct grand challenge. [Online] (2017), available: <http://www.aapm.org/GrandChallenge/LowDoseCT/>

2. Chen, T., Liu, G.H., Theodorou, E.A.: Likelihood training of schrödinger bridge using forward-backward sdes theory. arXiv preprint arXiv:2110.11291 (2021)
3. Chen, Y., Georgiou, T.T., Pavon, M.: Stochastic control liaisons: Richard sinkhorn meets gaspard monge on a schrodinger bridge. *Siam Review* **63**(2), 249–313 (2021)
4. Chung, H., Kim, J., Ye, J.C.: Direct diffusion bridge using data consistency for inverse problems. *Advances in Neural Information Processing Systems* **36** (2024)
5. De Bortoli, V., Thornton, J., Heng, J., Doucet, A.: Diffusion schrödinger bridge with applications to score-based generative modeling. *Advances in Neural Information Processing Systems* **34**, 17695–17709 (2021)
6. Delbracio, M., Milanfar, P.: Inversion by direct iteration: An alternative to denoising diffusion for image restoration. arXiv preprint arXiv:2303.11435 (2023)
7. Haralick, R.M., Shanmugam, K., Dinstein, I.H.: Textural features for image classification. *IEEE Transactions on systems, man, and cybernetics* **3**(6), 610–621 (1973)
8. Ho, J., Jain, A., Abbeel, P.: Denoising diffusion probabilistic models. *Advances in neural information processing systems* **33**, 6840–6851 (2020)
9. Jabri, A., Fleet, D., Chen, T.: Scalable adaptive computation for iterative generation. arXiv preprint arXiv:2212.11972 (2022)
10. Li, H., Yang, Y., Chang, M., Chen, S., Feng, H., Xu, Z., Li, Q., Chen, Y.: Srdiff: Single image super-resolution with diffusion probabilistic models. *Neurocomputing* **479**, 47–59 (2022)
11. Liu, G.H., Vahdat, A., Huang, D.A., Theodorou, E.A., Nie, W., Anandkumar, A.: I²sb: Image-to-image schrödinger bridge. arXiv preprint arXiv:2302.05872 (2023)
12. Saharia, C., Ho, J., Chan, W., Salimans, T., Fleet, D.J., Norouzi, M.: Image super-resolution via iterative refinement. *IEEE Transactions on Pattern Analysis and Machine Intelligence* **45**(4), 4713–4726 (2022)
13. Song, J., Meng, C., Ermon, S.: Denoising diffusion implicit models. arXiv preprint arXiv:2010.02502 (2020)
14. Wang, X., Xie, L., Dong, C., Shan, Y.: Real-esrgan: Training real-world blind super-resolution with pure synthetic data. In: *Proceedings of the IEEE/CVF international conference on computer vision*. pp. 1905–1914 (2021)
15. Wu, D., Kim, K., El Fakhri, G., Li, Q.: Iterative low-dose ct reconstruction with priors trained by artificial neural network. *IEEE transactions on medical imaging* **36**(12), 2479–2486 (2017)
16. Yu, P., Zhang, H., Kang, H., Tang, W., Arnold, C.W., Zhang, R.: Rplhr-ct dataset and transformer baseline for volumetric super-resolution from ct scans. In: *International Conference on Medical Image Computing and Computer-Assisted Intervention*. pp. 344–353. Springer (2022)